PNAS RESEARCH ARTICLE | IMMUNOLOGY AND INFLAMMATION

Alum-anchored intratumoral retention improves the tolerability and antitumor efficacy of type I interferon therapies

Emi A. Lutz[a,b], Yash Agarwal[a,b], Noor Momin[a,b], Sarah C. Cowles[a,c], Joseph R. Palmeri[a,c], Ellen Duong[a,d], Vladlena Hornet[a,b], Allison Sheen[a,b], Brianna M. Lax[a,c], Adrienne M. Rothschilds[a,b], Darrell J. Irvine[a,b,e,f,g,h], Stefani Spranger[a,d,f], and K. Dane Wittrup[a,b,c,1]

Edited by K. Garcia, Stanford University, Stanford, CA; received April 5, 2022; accepted July 11, 2022

Effective antitumor immunity in mice requires activation of the type I interferon (IFN) response pathway. IFNα and IFNβ therapies have proven promising in humans, but suffer from limited efficacy and high toxicity. Intratumoral IFN retention ameliorates systemic toxicity, but given the complexity of IFN signaling, it was unclear whether long-term intratumoral retention of type I IFNs would promote or inhibit antitumor responses. To this end, we compared the efficacy of IFNα and IFNβ that exhibit either brief or sustained retention after intratumoral injection in syngeneic mouse tumor models. Significant enhancement in tumor retention, mediated by anchoring these IFNs to coinjected aluminum-hydroxide (alum) particles, greatly improved both their tolerability and efficacy. The improved efficacy of alum-anchored IFNs could be attributed to sustained pleiotropic effects on tumor cells, immune cells, and nonhematopoietic cells. Alum-anchored IFNs achieved high cure rates of B16F10 tumors upon combination with either anti-PD-1 antibody or interleukin-2. Interestingly however, these alternative combination immunotherapies yielded disparate T cell phenotypes and differential resistance to tumor rechallenge, highlighting important distinctions in adaptive memory formation for combinations of type I IFNs with other immunotherapies.

interferon | cancer | intratumoral | alum | immunotherapy

Type I interferons (IFNs), comprising IFNα subtypes and IFNβ, are potent cytokines with significant impacts on antitumor immunity, angiogenesis, and tumor growth (1, 2). Endogenous type I IFNs are critical to antitumor immunity (3–5), and effective modulation of the type I IFN pathway holds great promise for improving cancer immunotherapies. Starting in the 1980s, IFNα gained approval from the US Food and Drug Administration (FDA) for the treatment of various cancers (6). IFNα is rapidly cleared, so extended half-life PEGylated IFNα was also FDA approved (7, 8). However, both IFNα and PEGylated IFNα suffer from low efficacy and high toxicity, in part because almost all cells in the body express the IFN-α/β receptor (IFNAR) (9). The challenges of type I IFN therapies have been recognized for decades, and there has been substantial effort to improve IFNs by tumor targeting (10–12), immune targeting (13, 14), and conditional activation at the tumor site (15–17), among other strategies (9).

We hypothesized that intratumorally injecting type I IFNs and retaining them in the tumor long term could improve on-target activity while reducing systemic toxicity. Intratumoral administration is feasible in the clinic (18–20), and local retention of other cytokines has safely promoted strong antitumor responses (21–23). In support of this hypothesis, inducing tumors to overexpress type I IFNs using gene transduction has enabled tumor regression in mice (24–27). On the other hand, some studies suggest that sustained IFN signaling in the tumor can be detrimental, particularly in the context of anti-PD-1 (αPD1) therapy (28–30). However, recombinant type I IFN therapies with long-term intratumoral retention have yet to be studied extensively in immunocompetent mice.

When intratumorally injecting cytokines, a retention strategy can prevent rapid leakage out of the tumor and thus maximize tumor exposure for improved efficacy (31). Recently, we anchored cytokines within tumors for weeks by introducing strong affinity to coinjected aluminum hydroxide (alum) particles (22). Alum is a safe, commonly used material that is FDA approved as a vaccine adjuvant. Agarwal et al. demonstrated in mice that alum-anchored interleukin-12 (IL-12) stayed at the tumor for weeks, reduced treatment-related toxicity, and promoted cures at primary tumors, metastases, and distant untreated lesions. Alum-anchoring enhanced the therapeutic efficacy of interleukin-2 (IL-2) as well (22).

In this article, we compared IFNα, extended half-life IFNα, and alum-anchored IFNα in syngeneic mouse tumor models. The impact of type I IFN subtype on treatment efficacy remains poorly defined (32–34), so we also developed IFNβ counterparts.

Significance

Type I IFNs hold considerable promise for the treatment of cancer, but it is unclear how best to activate this pathway pharmacologically. We compared the intratumoral administration of two type I IFN subtypes and three design strategies (IFN, extended half-life IFN, and intratumorally retained IFN) in several immunocompetent mouse tumor models. Intratumoral retention of type I IFNs greatly improved treatment efficacy and decreased toxicity. Intratumorally retained type I IFNs were also effective in combination immunotherapies. However, combination therapies with excessive cytokine signaling harmed adaptive memory formation. Intratumoral retention is a promising strategy for type I IFNs, but warrants careful consideration of IFN subtype, tumor phenotype, and agents for combination therapy.

Author contributions: E.A.L. and K.D.W. designed research; E.A.L., Y.A., N.M., S.C.C., J.R.P., E.D., V.H., A.S., B.M.L., and A.M.R. performed research; D.J.I. and S.S. contributed new reagents/analytic tools.; E.A.L., D.J.I., S.S., and K.D.W. analyzed data; and E.A.L. and K.D.W. wrote the paper.

Competing interest statement: Y.A., D.J.I., and K.D.W. are named as inventors in a patent application filed by the Massachusetts Institute of Technology related to the data presented in this work (US20200405950A1). D.J.I. and K.D.W. are co-founders of Ankyra Therapeutics, which has licensed rights to the intellectual property mentioned above.

This article is a PNAS Direct Submission.

[1]To whom correspondence may be addressed. Email: wittrup@mit.edu.

This article contains supporting information online at http://www.pnas.org/lookup/suppl/doi:10.1073/pnas.2205983119/-/DCSupplemental.

Published August 29, 2022.

Intratumoral retention improved the efficacy of type I IFNs as monotherapy. Optimal type I IFN subtype was context dependent. In combination with extended half-life IL-2, alum-anchored IFNs reduced toxicity and achieved high cure rates at the primary tumor, but suffered poor resistance to rechallenge tumors. When combined with αPD1, most IFN therapies were effective both at eliminating the primary tumor and protecting from subsequent tumor rechallenge. We investigated the mechanisms behind these therapeutic outcomes and discuss how these results can inform effective design strategies for type I IFN therapies.

Results

Development of a Panel of Type I IFNs. We developed five type I IFNs with different signaling strengths and pharmacokinetics (Fig. 1*A* and *SI Appendix*, Fig. S1 *A* and *B* and Table S1). We recombinantly expressed murine IFNα subtype A (referred to here as IFNα), and murine IFNβ, which is an order of magnitude more potent than IFNα (35). Since PEGylated IFNα is used in the clinic (7, 8), we also generated an extended half-life format of IFNα by fusion to mouse serum albumin (MSA). Albumin extends cytokine half-life by FcRn-mediated recycling and reducing renal clearance, and albumin-IFNα fusions have been previously validated (9, 36, 37).

Next, we employed a system that we recently developed to enable long-term retention of intratumorally injected cytokines (22). This strategy relies on aluminum hydroxide (alum) particles that are retained at their injection site as a physical depot for weeks. By fusion to an alum-binding peptide (ABP), ABP cytokines that are mixed and coinjected with alum are also retained long term. The design of ABP contains serine motifs that are phosphorylated upon coexpression with the Fam20C kinase (22) because phosphates bind tightly to alum through a ligand exchange reaction with surface hydroxyls (38, 39). Indeed, ABP-IFNs had higher phosphorylation (*SI Appendix*, Fig. S1*C*) and tighter alum binding (Fig. 1*B*) compared to IFNs without ABP. To test translatability, we confirmed that human IFNα2b could be expressed (*SI Appendix*, Fig. S1*D*) and phosphorylated (*SI Appendix*, Fig. S1*E*) as an ABP fusion. All five murine IFNs activated RAW-Lucia Interferon-stimulated genes (ISG) cells, an IFN-responsive macrophage line, albeit with a mild increase in half maximal effective concentration (EC_{50}) for fusion proteins (Fig. 1*C*). IFNβ constructs were an order of

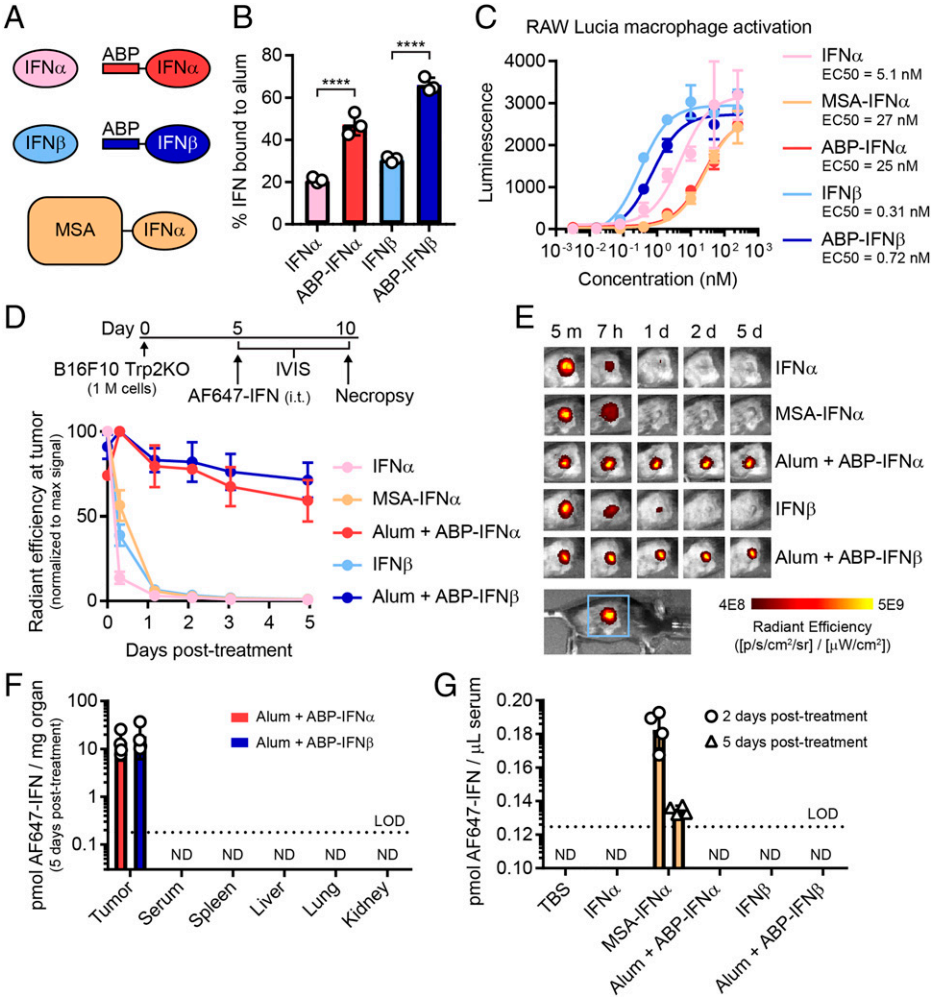

Fig. 1. Activity and pharmacokinetics of IFNs. (*A*) Schematic of type I IFN fusion proteins. (*B*) Fluorescently labeled IFNs and alum were incubated for 20 min in TBS, then resuspended in PBS 10% mouse serum for 1 h. Fluorescence spectroscopy was used to measure the percentage of IFN that remained bound to alum; mean ± SD ($n = 3$). (*C*) RAW-Lucia ISG macrophage activation in response to IFNs; mean ± SD ($n = 3$). (*D*–*G*) Mice bearing subcutaneous B16F10 Trp2KO tumors were injected i.t. on day 5 with 0.5 nmol AF647-labeled IFNs and tracked by IVIS. (*D*) Total radiant efficiency at the tumor normalized to max signal; mean ± SD ($n = 4$). (*E*) Images of representative mice. The blue box shows the field of view around the tumor. m, minutes; h, hours; d, days. (*F* and *G*) AF647-IFN levels in (*F*) homogenized organs on day 10 and (*G*) serum on days 7 and 10, measured by fluorescence spectroscopy; mean ± SD ($n = 4$). ND, not detected; LOD, limit of detection. Statistics: comparisons generated by one-way ANOVA with Tukey's multiple comparisons test. ****$P < 0.0001$.

magnitude more potent than IFNα constructs, and ABP-IFNs maintained their activity in the presence of alum (*SI Appendix*, Fig. S1*F*).

To evaluate pharmacokinetics, we injected AF647-labeled IFNs intratumorally (i.t.) into apigmented B16F10 tumors and tracked their retention at the tumor for 5 d (Fig. 1 *D* and *E*). Upon coinjection with alum, ABP-IFNα and ABP-IFNβ were retained in the tumor for all 5 d. In contrast, IFNα, IFNβ, and MSA-IFNα leaked out of the tumor within 1 d. Five days after treatment, AF647-IFN levels in homogenized organs were measured by fluorescence spectroscopy. ABP-IFNs were highly specific for the tumor, with no signal detected in the serum, spleen, liver, lung, or kidney (Fig. 1*F*). Serum fluorescence levels confirmed that MSA-IFNα had extended circulation, while the other IFNs were not detected in the serum at the time points tested (Fig. 1*G*).

Intratumoral Retention Improves Type I IFN Monotherapy. The five IFNs were tested for therapeutic efficacy as a single agent. Mice bearing established MC38 colon carcinoma tumors or B16F10 melanoma tumors were treated with 0.5 nmol IFN i.t. on days 5, 11, and 17. Survival (Fig. 2 *A* and *B*) and tumor growth (Fig. 2*C* and *SI Appendix*, Fig. S2 *A* and *B*) demonstrated that IFNα had poor efficacy in both tumor models and only extended median survival by 4 to 5 d compared to the Tris-buffered saline (TBS) control. IFNβ was not significantly different from IFNα ($P = 0.18$ for MC38, $P = 0.81$ for B16F10), indicating that increasing signaling strength alone was insufficient to improve efficacy.

Intratumoral retention improved survival from type I IFN therapies. Alum + ABP-IFNα significantly extended survival over IFNα ($P = 0.0005$ for MC38, $P = 0.01$ for B16F10). Similarly, alum + ABP-IFNβ was more efficacious than IFNβ ($P = 0.0005$ for MC38, $P < 0.0001$ for B16F10). As a control, even large doses of alum alone did not slow tumor growth, indicating that the efficacy was IFN mediated (*SI Appendix*, Fig. S2*C*) (22).

In immunologically cold B16F10 tumors, the more potent alum + ABP-IFNβ was more efficacious than alum + ABP-IFNα ($P = 0.004$). In contrast, in the MC38 model, the less potent alum + ABP-IFNα was more efficacious than alum + ABP-IFNβ ($P = 0.002$). MC38 tumors have higher basal type I IFN signaling and immune infiltration compared to B16F10 tumors (40–42). There may be a threshold for productive type I IFN signaling, and overactivation may be detrimental in tumors with preexisting high IFN signatures. Consistent with this hypothesis, $CD8^+$ T cells in MC38 tumors treated with alum + ABP-IFNβ had high levels of exhaustion marker TIM3 and suppressive marker PD-L1 (*SI Appendix*, Fig. S3*A*) (43, 44). Optimal type I IFN signaling is complex and tumor dependent.

MSA-IFNα had similar efficacy to alum + ABP-IFNα in both models ($P = 0.48$ for MC38, $P = 0.43$ for B16F10). However, mice treated with MSA-IFNα experienced mild body weight loss on day 7 that was not observed from the alum-anchored IFNs, raising potential toxicity concerns for prolonging half-life without intratumoral retention (Fig. 2*D* and *SI Appendix*, Fig. S2*B*). Intraperitoneal (i.p.) treatments of the same MSA-IFNα dose had poor efficacy in B16F10-bearing mice (*SI Appendix*, Fig. S3*B*), indicating that intratumoral exposure is key to type I IFN efficacy.

Next, we asked how intratumoral retention improved type I IFN therapies. We focused on the poorly inflamed B16F10 model because type I IFNs are particularly promising for turning cold tumors hot (5). We also focused on alum + ABP-IFNβ because this had the strongest efficacy in B16F10 tumors (Fig. 2 *B* and *C*). Type I IFNs are pleiotropic and can have a wide range of impacts on tumor cells, endothelial cells, and immune cells (1, 2). We examined each of these compartments to uncover the therapeutic mechanism behind alum + ABP-IFNβ in B16F10 tumors.

Alum + ABP-IFNβ Therapy Alters Tumor Cells. To study impacts on tumor cells, B16F10 tumors were treated with TBS, IFNβ, or alum + ABP-IFNβ, followed 4 d later by flow cytometry of live tumor cells (Fig. 3*A* and *SI Appendix*, Fig. S4*A*). In addition to wild-type (WT) mice, we included Ifnar1$^{-/-}$ mice whose host cells are deficient in type I IFN sensing, so only the implanted B16F10 cells can directly respond to IFN treatment.

Type I IFNs can alter how tumor cells interact with immune cells via transcriptional regulation of thousands of genes (2). Importantly, type I IFNs up-regulate major histocompatibility complex I (MHC-I) on tumor cells, improving immune recognition (45). Alum + ABP-IFNβ led to a greater proportion of B16F10 cells with high MHC-I expression in both WT mice ($P = 0.04$ compared to TBS) and Ifnar1$^{-/-}$ mice ($P = 0.009$ compared to TBS) (Fig. 3*B* and *SI Appendix*, Fig. S4*B*). The

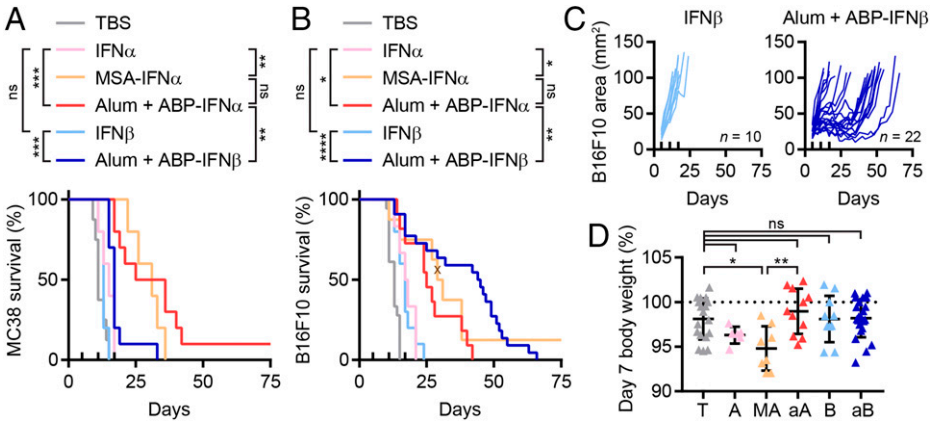

Fig. 2. Intratumoral retention improves IFN monotherapy. Mice were inoculated on day 0 with (*A*) 1 M MC38 cells or (*B–D*) 1 M B16F10 cells subcutaneously. Mice were treated i.t. on days 5, 11, and 17 (ticks above *x* axis) with TBS or 0.5 nmol IFN. MC38 study: TBS (T), $n = 8$; MSA-IFNα (MA), IFNα (A), and IFNβ (B), $n = 5$; alum + ABP-IFNα (aA) and alum + ABP-IFNβ (aB), $n = 10$. B16F10 study: T, $n = 18$; MA, $n = 8$; A, $n = 6$; B, $n = 10$; aA, $n = 11$; and aB, $n = 22$. (*A* and *B*) Survival. "x" marks killing from poor body condition. (*C*) Individual tumor growth for indicated groups in the B16F10 study. (*D*) Day 7 body weight normalized to the start of treatment (day 5) for the B16F10 study; mean ± SD. Statistics: survival compared by log-rank Mantel–Cox test. Weights compared by one-way ANOVA with Tukey's multiple comparisons test. ns, not significant; *$P < 0.05$; **$P < 0.01$; ***$P < 0.001$; ****$P < 0.0001$.

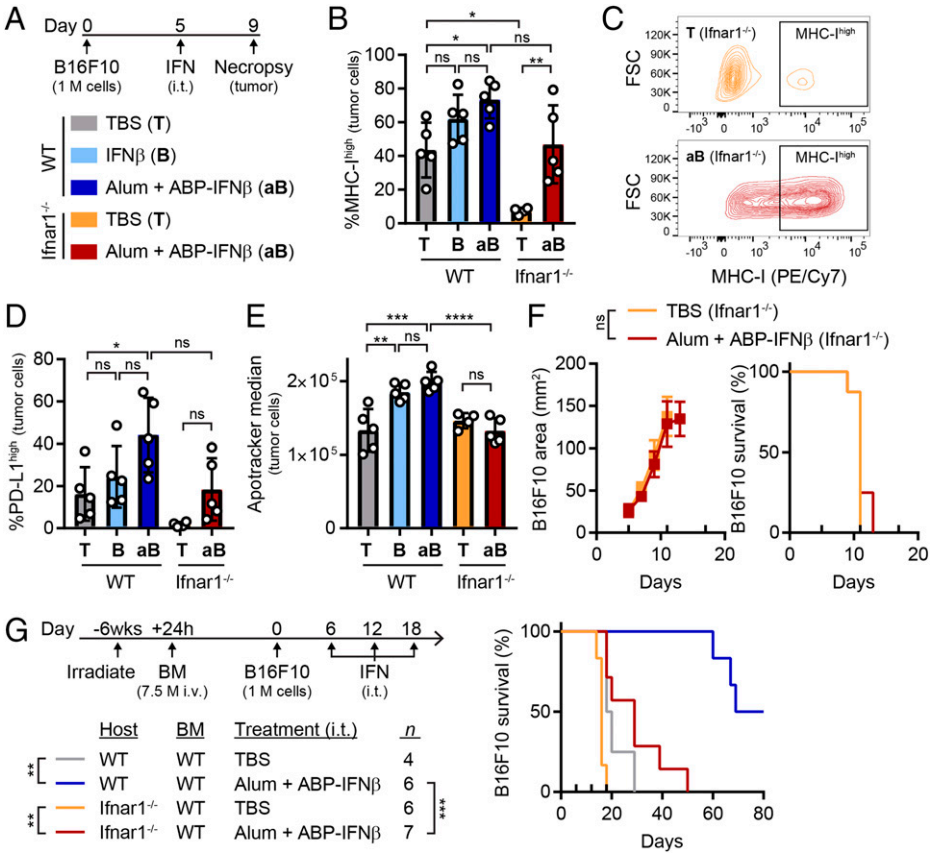

Fig. 3. Alum + ABP-IFNβ engages with tumor cells and nonhematopoietic cells. (*A–E*) WT and Ifnar1$^{-/-}$ mice were inoculated on day 0 with 1 M B16F10 cells and treated i.t. on day 5 with TBS, IFNβ, or alum + ABP-IFNβ. On day 9, tumors were excised and analyzed by flow cytometry. TBS-treated Ifnar1$^{-/-}$ mice, $n = 4$; other groups, $n = 5$. (*A*) Timeline. (*B*) Percentage of live tumor cells that were MHC-I^{high}. (*C*) Representative flow data (5% contour plots) for Ifnar1$^{-/-}$ mice treated with TBS or alum + ABP-IFNβ. (*D*) Percentage of live tumor cells that were PD-L1^{high}. (*E*) Median Apotracker Green levels of live tumor cells. (*F*) Tumor growth (mean ± SD) and survival of Ifnar1$^{-/-}$ mice inoculated on day 0 with 1 M B16F10 cells and treated i.t. on days 5 and 11 (ticks above *x* axis) with TBS or alum + ABP-IFNβ ($n = 8$). All tumors exceeded 100 mm^2 before the typical third dose. (*G*) WT and Ifnar1$^{-/-}$ hosts were lethally irradiated, followed by BM transplant from WT donors. After 6 wk, engraftment was confirmed. Survival is shown for mice inoculated with 1 M B16F10 cells on day 0, then treated i.t. with TBS or alum + ABP-IFNβ on days 6, 12, and 18 (ticks above *x* axis); *n* indicated on plot. Statistics: survival compared by log-rank Mantel–Cox test. Other comparisons generated by one-way ANOVA with Tukey's multiple comparisons test. ns, not significant; *$P < 0.05$; **$P < 0.01$; ***$P < 0.001$; ****$P < 0.0001$.

altered MHC-I phenotype was substantial even in Ifnar1$^{-/-}$ mice (Fig. 3 *B* and *C*), suggesting that alum-anchored payloads were unexpectedly uniformly accessible throughout the tumor. TBS-treated WT mice had higher MHC-I levels than TBS-treated Ifnar1$^{-/-}$ mice ($P = 0.02$, Fig. 3*B*), highlighting that endogenous type I IFN signaling also impacts B16F10 cells considerably in this therapy. Type I IFNs can also up-regulate PD-L1 on tumor cells, which suppresses T cell function by binding to the PD-1 receptor expressed on activated T cells (12). Alum + ABP-IFNβ increased the percentage of B16F10 cells with high PD-L1 expression ($P = 0.03$ compared to TBS) (Fig. 3*D* and *SI Appendix*, Fig. S4*C*). Although not significant, PD-L1 levels also trended upwards in treated Ifnar1$^{-/-}$ mice.

Type I IFNs can be antiproliferative and proapoptotic to tumor cells (2). No antiproliferative activity was observed in tumor cells as measured by Ki67 (*SI Appendix*, Fig. S4*D*). However, alum + ABP-IFNβ caused live tumor cells in WT mice to be more apoptotic, as measured by Apotracker Green, which detects phosphatidylserine residues on the cell surface ($P = 0.0001$ compared to TBS, Fig. 3*E*). No changes in Apotracker Green levels occurred in Ifnar1$^{-/-}$ mice ($P = 0.77$), indicating that the proapoptotic effect observed in WT mice was mediated indirectly.

This study showed that alum + ABP-IFNβ altered tumor cells, both directly (MHC-I and PD-L1 levels) and indirectly (apoptosis). The direct effects on tumor cells were impactful and led to an increase in total CD45$^+$ immune cells in the tumor in Ifnar1$^{-/-}$ mice (*SI Appendix*, Fig. S4 *E* and *F*). However, the direct effects on tumor cells alone were insufficient to slow tumor growth. The strong efficacy of alum + ABP-IFNβ in WT mice (Fig. 2*B*) was completely lost when the treatment regimen was repeated in Ifnar1$^{-/-}$ mice (Fig. 3*F*), indicating that interactions with IFN-responsive host cells are essential for efficacy.

Alum + ABP-IFNβ Therapy Relies on Nonhematopoietic Cells. Endothelial cells are an important consideration because type I IFNs are antiangiogenic (1, 24). In order to examine the role of nonhematopoietic cells in treatment efficacy, bone marrow chimeras were generated. WT and Ifnar1$^{-/-}$ hosts were lethally irradiated, then reconstituted with bone marrow (BM) from congenically marked WT donors. Thus, in the Ifnar1$^{-/-}$ hosts, the nonimmune compartment is deficient in type I IFN sensing. After 6 wk, BM engraftment was confirmed (*SI Appendix*, Fig. S5*A*). Mice were inoculated with B16F10 tumors, followed by TBS or alum + ABP-IFNβ treatments. As expected, survival (Fig. 3*G*) and tumor growth (*SI Appendix*, Fig. S5*B*) showed strong therapeutic efficacy in WT hosts ($P = 0.001$). The treatment still promoted tumor growth delay and extended survival in Ifnar1$^{-/-}$ hosts ($P = 0.001$). However, comparing the two

alum + ABP-IFNβ groups revealed significant reduction in efficacy by removing the nonhematopoietic compartment's ability to respond to type I IFNs ($P = 0.0004$).

Alum + ABP-IFNβ Activates Dendritic Cells and CD8$^+$ T Cells. To begin assessing the immune compartment, B16F10 tumors were treated with TBS, IFNβ, or alum + ABP-IFNβ, and tumor lysates were analyzed 4 d later for chemokines and cytokines. All concentrations are reported (*SI Appendix*, Fig. S6), and a heatmap visualizes fold change compared to TBS (Fig. 4*A*). Compared to TBS, alum + ABP-IFNβ significantly increased CXCL10 (14-fold, $P < 0.0001$), IFNγ (7.4-fold, $P = 0.0009$), RANTES (5.8-fold, $P < 0.0001$), MCP-1 (3.2-fold, $P = 0.0002$), IL-12 (2.6-fold, $P = 0.0003$), IL-10 (1.7-fold, $P = 0.0009$), TNFα (1.7-fold, $P = 0.047$), IL-1β (1.5-fold, $P = 0.01$), and GM-CSF (1.4-fold, $P = 0.003$). Compared to unanchored IFNβ, alum + ABP-IFNβ had significantly higher CXCL10 ($P < 0.0001$), RANTES ($P = 0.001$), and MCP-1 ($P = 0.001$), highlighting that intratumoral retention induced a stronger chemokine signature.

To understand which immune cells play a role, the alum + ABP-IFNβ treatment regimen was repeated using mice lacking specific immune compartments via genetic knockout or confirmed antibody-mediated depletions (*SI Appendix*, Fig. S7*A*). Depleting natural killer (NK) cells and neutrophils did not harm efficacy (*SI Appendix*, Fig. S7*B*). The Nlrp3 inflammasome, which can be activated by alum, was also dispensable (*SI Appendix*, Fig. S7*C*) (46). However, treatment efficacy was significantly reduced in mice lacking Batf3 dendritic cells (DCs) ($P = 0.0002$) or CD8$^+$ T cells ($P = 0.0003$) (Fig. 4*B*). The type I IFN pathway plays a pivotal role in DC antigen presentation and CD8$^+$ T cell priming and expansion (3–5). Indeed, 4 d after treatment with alum + ABP-IFNβ, there was a greater proportion (Fig. 4*C*) and total count (*SI Appendix*, Fig. S7*D*) of Ly6C$^-$ MHCII$^+$ CD24$^+$ DCs in the tumor draining lymph node (tdLN) that expressed activation marker CD86. In addition, 6 d after treatment with alum + ABP-IFNβ, there were more CD8$^+$ T cells per milligram of tumor (*SI Appendix*, Fig. S7*E*) and a greater proportion of CD8$^+$ T cells in the tumor were activated compared to TBS, as measured by Ki67 ($P = 0.003$), TIM3 ($P = 0.002$), and TCF1 ($P = 0.01$) (Fig. 4*D* and *SI Appendix*, Fig. S7*E*).

These experiments revealed a pleiotropic mechanism of action in B16F10 tumors. Alum + ABP-IFNβ induced important changes in tumor cells, and therapeutic efficacy relied on multiple contributions from nonhematopoietic cells, DCs, and CD8$^+$ T cells. After investigating how alum + ABP-IFNβ interacted with the tumor microenvironment as a single agent, we moved on to study whether combining IFNs with other immunotherapies could enable tumor cures.

IFNs in Combination with MSA-IL2 or αPD1. First, we combined the panel of IFNs with an extended half-life form of IL-2 (MSA-IL2) (47). IFNα and IL-2 are currently the only FDA-approved cytokines for cancer. Although IFNα and IL-2 play complementary roles in the cancer immunity cycle (48–50), their combination has been generally unsuccessful in the clinic to date (51–53). B16F10 tumors were treated on days 5, 11, and 17 with IFNs (i.t.), previously shown not to be curative as a single agent (Fig. 2*B*). Thirty micrograms of MSA-IL2 (i.p.) was dosed concurrently. Survival (Fig. 5*A*) and tumor growth (*SI Appendix*, Fig. S8*A*) showed that MSA-IL2 alone delayed median survival by only 2 d. Almost complete cure rates were achieved when MSA-IL2 was combined with alum + ABP-IFNα (6/6 cures) or alum + ABP-IFNβ (6/7 cures). In stark contrast, no mice were cured when MSA-IL2 was combined with IFNα,

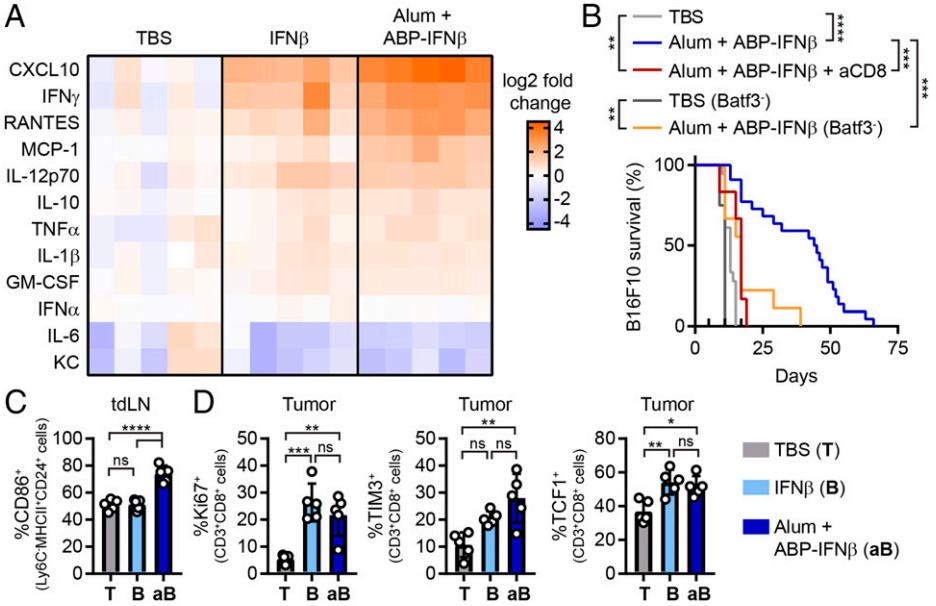

Fig. 4. Alum + ABP-IFNβ activates DCs and CD8$^+$ T cells. All mice were inoculated on day 0 with 1 M B16F10 cells. (*A*) Mice were treated i.t. on day 5 with TBS, IFNβ, or alum + ABP-IFNβ, and day 9 tumor lysates were analyzed for cytokines and chemokines. Heatmap columns show data from individual mice ($n = 5$), reported as log2 fold change in concentration compared to the average value of the TBS group. Raw data are in *SI Appendix*, Fig. S6. (*B*) Survival of WT and Batf3$^{-/-}$ mice treated i.t. with TBS or alum + ABP-IFNβ on days 5, 11, and 17 (ticks above *x* axis). Some mice received aCD8-depleting antibody every 4 d. WT mice: TBS, $n = 18$; alum + ABP-IFNβ, $n = 22$; alum + ABP-IFNβ + aCD8, $n = 6$. Batf3$^{-/-}$ mice: TBS, $n = 8$; alum + ABP-IFNβ, $n = 9$. (*C*) B16F10-bearing mice were treated i.t. on day 5 with TBS, IFNβ, or alum + ABP-IFNβ. On day 9, tumor-draining lymph nodes were excised and analyzed via flow cytometry for the percentage of Ly6C$^-$ MHCII$^+$ CD24$^+$ DCs that were CD86$^+$; mean ± SD ($n = 5$). (*D*) B16F10-bearing mice were treated i.t. on day 5 with TBS, IFNβ, or alum + ABP-IFNβ. On day 11, tumors were excised and analyzed via flow cytometry for the percentage of CD3$^+$ CD8$^+$ T cells that were Ki67$^+$, TIM3$^+$, and TCF1$^+$; mean ± SD ($n = 5$). Statistics: survival compared by log-rank Mantel–Cox test. Other comparisons generated by one-way ANOVA with Tukey's multiple comparisons test. ns, not significant; *$P < 0.05$; **$P < 0.01$; ***$P < 0.001$; ****$P < 0.0001$.

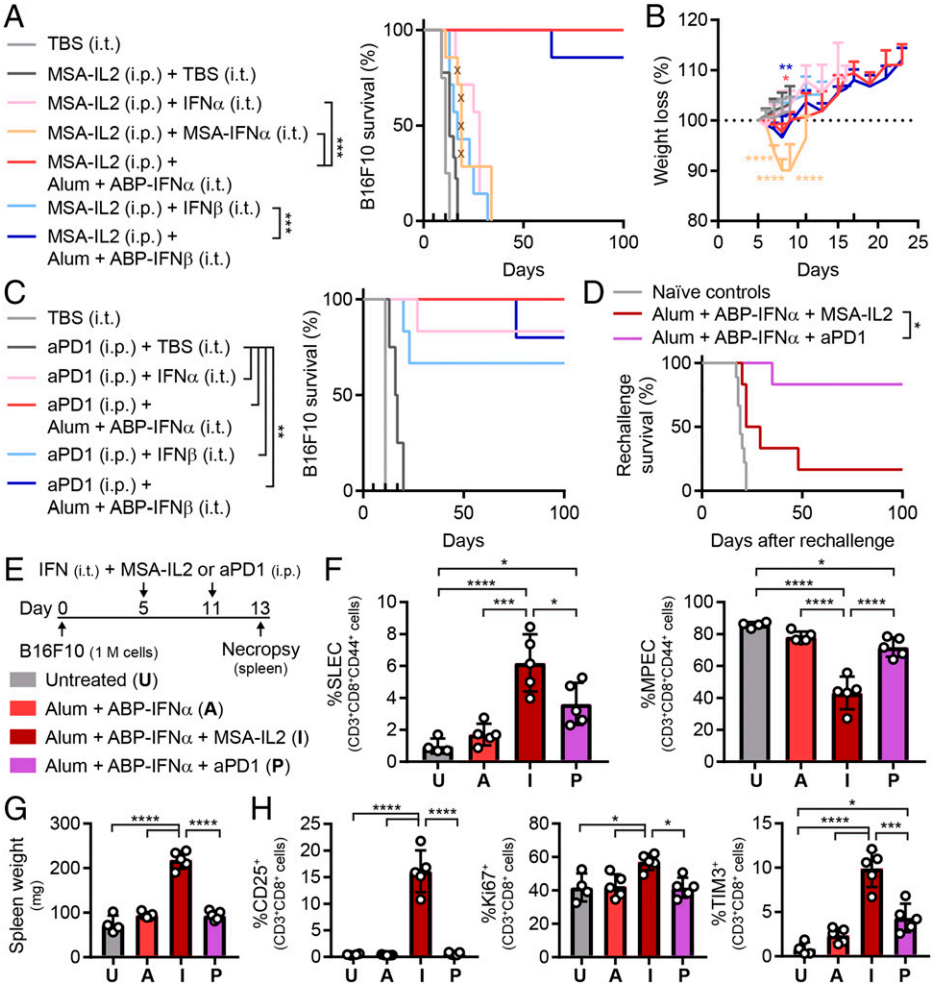

Fig. 5. Combination therapies have contrasting memory responses. All mice were inoculated on day 0 with 1 M B16F10 cells. (*A* and *B*) Mice were treated on days 5, 11, and 17 (ticks above *x* axis) with MSA-IL2 (i.p.) and IFN (i.t.). TBS, $n = 8$; MSA-IL2 + TBS, $n = 9$; other groups, $n = 6$ or 7. (*A*) Survival. "x" marks killing from poor body condition or weight loss. (*B*) Body weight normalized to day 5 until a mouse in that group was killed; mean + SD. Statistics show comparisons to TBS. (*C*) Mice were treated on days 5, 11, and 17 with αPD1 (i.p.) and IFN (i.t.). αPD1 + TBS, $n = 4$; other groups, $n = 5$ or 6. (*D*) Survival of naïve controls ($n = 9$), alum + ABP-IFNα + MSA-IL2 cures ($n = 6$), and alum + ABP-IFNα + αPD1 cures ($n = 6$) rechallenged with 0.1 M B16F10 cells. (*E* to *H*) B16F10-bearing mice were treated on days 5 and 11 with alum + ABP-IFNα (i.t.) and MSA-IL2 or αPD1 (i.p.). On day 13, spleens were excised. Untreated, $n = 4$; other groups, $n = 5$. (*E*) Timeline. (*F*) Proportion of $CD127^-$ $KLRG1^+$ SLECs and $CD127^+$ $KLRG1^-$ MPECs out of $CD3^+$ $CD8^+$ $CD44^+$ cells. (*G*) Spleen weight. (*H*) Proportion of $CD25^+$, $Ki67^+$, and $TIM3^+$ out of $CD3^+$ $CD8^+$ cells. Statistics: survival compared by log-rank Mantel–Cox test. Two-way ANOVA (weights) or one-way ANOVA (other comparisons) with Tukey's multiple comparisons test was used. $^*P < 0.05$; $^{**}P < 0.01$; $^{***}P < 0.001$; $^{****}P < 0.0001$.

MSA-IFNα, or IFNβ. However, we and others have observed that cytokine combinations can exacerbate treatment-related toxicities (21, 54, 55). Extended half-life MSA-IFNα combined with MSA-IL2 led to substantial weight loss, and four out of seven mice were killed due to toxicity (Fig. 5*B*). In contrast, alum-localized IFNs combined with MSA-IL2 avoided this overt toxicity.

Second, we combined IFNs with αPD1, in part motivated by the PD-L1 up-regulation on tumor cells following localized IFN treatment (Fig. 3*D* and *SI Appendix*, Fig. S4*C*). There are also reports of improved antitumor efficacy in mice from combining type I IFN pathway agonists with αPD1 or αPD-L1 (11, 12, 56). Mice bearing B16F10 tumors were treated on days 5, 11, and 17 with IFNs (i.t.) and 200 μg αPD1 (i.p.). Survival (Fig. 5*C*) and tumor growth (*SI Appendix*, Fig. S8*B*) demonstrated that αPD1 alone could not cure B16F10 tumors. Mice were cured when αPD1 was combined with IFNα (5/6 cures), alum + ABP-IFNα (6/6 cures), IFNβ (4/6 cures), or alum + ABP-IFNβ (4/5 cures). Mice did not lose weight (*SI Appendix*, Fig. S8*B*).

Combination Immunotherapies Yield Contrasting Memory Responses. After 100 to 110 d, cured mice were rechallenged with 0.1 M B16F10 cells in the opposite flank and monitored for an additional 100 d. We observed poor resistance to rechallenge in mice cured from MSA-IL2 combined with alum + ABP-IFNα (1/6 survivors) or alum + ABP-IFNβ (1/6 survivors) (*SI Appendix*, Fig. S8*C*). Mice cured from αPD1 + alum + ABP-IFNβ also had poor resistance to rechallenge (1/4 survivors) (*SI Appendix*, Fig. S8*D*). In contrast, we observed strong resistance to rechallenge in mice cured from αPD1 combined with IFNα (4/5 survivors), IFNβ (4/4 survivors), or alum + ABP-IFNα (5/6 survivors) (*SI Appendix*, Fig. S8*D*). We were specifically intrigued by the difference between alum + ABP-IFNα in combination with MSA-IL2 compared to αPD1. Both therapies achieved 100% cures at the primary tumor (Fig. 5 *A* and *C*) but led to starkly different resistance to rechallenge ($P = 0.02$) (Fig. 5*D*).

To investigate this mechanism, B16F10 tumors were treated on days 5 and 11 with alum + ABP-IFNα, either alone, with MSA-IL2, or with αPD1 (Fig. 5*E*). On day 13, spleens were

excised, and T cells were analyzed by flow cytometry (*SI Appendix*, Fig. S9*A*). Markers KLRG1 and CD127 (a subunit of IL-7R) predict if $CD8^+$ T cells are short-lived effector cells (SLECs) or memory precursor effector cells (MPECs) (57–60). Alum + ABP-IFNα alone did not appreciably raise the percentage of $CD3^+$ $CD8^+$ $CD44^+$ effector T cells that were SLECs (%SLECs), which may explain why alum + ABP-IFNα failed to achieve cures as a single agent (Fig. 5*F* and *SI Appendix*, Fig. S9 *B* and *C*). In contrast, the MSA-IL2 combination substantially increased %SLECs ($P < 0.0001$ compared to untreated), helping explain the 6/6 cure rate at the primary tumor. However, the increase in %SLECs came at the cost of a drastic decrease in %MPECs ($P < 0.0001$ compared to untreated), consistent with the poor rechallenge results from the MSA-IL2 combination. On the other hand, the αPD1 combination increased %SLECs compared to untreated ($P = 0.03$), but to a lesser extent than the MSA-IL2 combination ($P = 0.02$). Conversely, the αPD1 combination had mild reduction in %MPECs compared to untreated ($P = 0.03$), but still maintained high %MPECs compared to the MSA-IL2 combination ($P < 0.0001$).

The MSA-IL2 combination had several additional key differences compared to the αPD1 combination. The MSA-IL2 combination-treated mice had enlarged spleens ($P < 0.0001$) (Fig. 5*G*), although there was no significant increase in total $CD8^+$ T cells in the spleen (*SI Appendix*, Fig. S10*A*) (61). The MSA-IL2 combination also increased the proportion of $CD8^+$ T cells that expressed CD25 ($P < 0.0001$), proliferation marker Ki67 ($P = 0.01$), and exhaustion marker TIM3 ($P = 0.0001$) (Fig. 5*H* and *SI Appendix*, Fig. S10*B*). Of note, excessive CD25 expression and prolonged IL-2 signaling have been reported to make T cells prone to terminal differentiation (62). All treatments increased TCF1 levels compared to untreated (*SI Appendix*, Fig. S10*C*). Overall, the MSA-IL2 combination with poor rechallenge data had spleens with a dramatic increase in SLECs, reduction in MPECs, and overactivation of T cells.

Discussion

Cytokines can initiate potent antitumor immune responses, but their use is hindered by poor therapeutic indices (9). Systemic delivery of cytokines is challenging because cytokine receptors are widely expressed throughout the body, leading to high receptor engagement in the periphery, even if tumor targeting is attempted (63). Consequently, a growing body of cytokine therapeutic development has begun shifting from systemic to intratumoral administration. Local delivery enables high cytokine concentration at the tumor initially, but unanchored proteins can rapidly leak out (31). Strategies that afford some retention to locally injected cytokines include tethering to the extracellular matrix (21, 23, 31, 64), cellular targets (65–67), or various biomaterials (68–70). Of note, we recently enabled particularly long-term intratumoral retention for weeks by using the FDA-approved material alum, which forms intratumoral depots and serves as an anchor for alum-binding cytokines (22). Together, these strategies have demonstrated that intratumorally injecting and retaining cytokines like IL-2, IL-12, and TNF can dramatically improve toxicity and initiate potent systemic antitumor immunity. However, it was unclear whether recombinant type I IFNs would similarly benefit from intratumoral retention in immunocompetent mice. In the present work, we engineered intratumorally retained IFNs and characterized their therapeutic potential and mechanism.

We developed five IFNs with different signaling strengths and pharmacokinetics: IFNα, IFNβ, extended half-life MSA-IFNα, alum-anchored ABP-IFNα, and alum-anchored ABP-IFNβ. Compared to IFNα or IFNβ alone, alum-anchored IFNs improved antitumor efficacy as an MC38 monotherapy, B16F10 monotherapy, and B16F10 combination therapy with MSA-IL2. When combined with αPD1, all IFNs tested exhibited a high B16F10 cure rate. Extended half-life IFNα is also clinically relevant (7, 8). Extended half-life MSA-IFNα was efficacious and tolerated as a single agent in mice. However, the combination setting with MSA-IL2 brought out benefits from alum-anchored IFNs, both in terms of survival and weight loss. These results show that alum anchoring enabled high efficacy from type I IFNs while maintaining safe tolerability in mice.

We examined the mechanism behind alum + ABP-IFNβ monotherapy in B16F10 tumors in detail. With regards to tumor cells, others have observed that hydrogel-retained human IFNα moderately slowed the growth of xenograft tumors in nude mice (71–74), and tumors exhibited decreased proliferation and increased apoptosis in vivo (71, 72). In our immunocompetent tumor model, alum-anchored IFNβ did not directly slow the growth of B16F10 tumors, but did indirectly increase apoptosis on tumor cells. Alum-anchored IFNβ also led to tumors up-regulating MHC-I, which improves immune recognition, and up-regulating PD-L1, which increases the likelihood of T cell exhaustion. We did not test other potential impacts of IFNs on tumor cells, such as altering the cell cycle or the epithelial-to-mesenchymal transition (2).

Alum-anchored IFNβ heavily relied on nonhematopoietic cells for efficacy. A previous study also observed the importance of nonhematopoietic cells for local IFNβ. Gajewski and coworkers generated B16 tumor cells that overexpressed IFNβ, which caused tumors to regress (24). Regression depended on IFNAR expression in vascular endothelial cells. Consistent with type I IFN's antiangiogenic properties (1), IFNβ-expressing B16 tumors had lower blood vessel density (24). Type I IFNs can also cause endothelial cells to produce chemokines like CXCL10 that play roles in inhibiting angiogenesis, as well as in recruiting and activating immune cells (75, 76). We indeed observed much higher CXCL10 levels from alum-anchored IFNβ compared to unanchored IFNβ, although we did not directly measure blood vessel density.

Another component of alum-anchored IFNβ's mechanism was immune mediated. Alum + ABP-IFNβ elicited a strong inflammatory signature with increased levels of many cytokines and chemokines at the tumor. Batf3 DCs and $CD8^+$ T cells were critical to therapy, both of which had improved activation upon treatment, consistent with the role of type I IFNs in DC antigen presentation and $CD8^+$ T cell priming and expansion (3–5). Although we investigated the major immune cells implicated in IFN therapies, including DCs, $CD8^+$ T cells, NK cells, and neutrophils, studying additional cell types like Tregs and macrophages may reveal additional mechanisms (1, 2). We also did not directly test which immune cells require type I IFN signaling.

Overall, alum-anchored IFNβ orchestrated a pleiotropic mechanism of action with impacts on tumor cells, nonhematopoietic cells, and immune cells. The complex downstream effects of alum-anchored IFN cooperated here to generally achieve significant antitumor efficacy. Nevertheless, the inherent pleiotropic nature of cytokines can be challenging in the clinic (9). Alum anchoring offers a way to confine cytokine pleiotropy in a spatial manner by concentrating effects to the tumor microenvironment. Others have constrained IFN pleiotropy at a cellular level by reducing IFN signaling strength such that it is effective only if a

coupled targeting moiety localizes the attenuated cytokine to a cell of interest (13, 14). Further control of IFN pleiotropy may be achieved by using both spatial and cellular strategies to constrain IFN signaling.

Alum-anchored IFNs in combination with MSA-IL2 or αPD1 were highly efficacious at the primary tumor, but had distinct response to rechallenge tumors, which could be explained by T cell phenotypes in the periphery (57–62). T cells exposed to alum-anchored IFNs can be enhanced by a secondary agent, but overactivation renders them useless in a rechallenge setting. Alum-anchored IFNα combined with MSA-IL2 had poor resistance to rechallenge, correlating with a drastic increase in SLECs, reduced MPECs, and excessive T cell activation. In contrast, alum-anchored IFNα combined with αPD1 had strong resistance to rechallenge. Further investigation is needed to see whether an effective balance between MPECs and SLECs can be regained for the IL-2 combination by reducing the MSA-IL2 dose or by using tumor-localized IL-2. It will also be useful to extend these studies to abscopal tumors and metastases, which may require a different balance of MPECs, SLECs, and tumor specificity.

Throughout this work, testing IFNs with different signaling strengths revealed further nuances of type I IFN therapies. IFNα and IFNβ performed similarly in all settings. However, alum + ABP-IFNα differed from alum + ABP-IFNβ in a few contexts. As a B16F10 monotherapy, the more potent alum + ABP-IFNβ had the highest efficacy. In contrast, as an MC38 monotherapy, alum + ABP-IFNβ had inferior efficacy and $CD8^+$ T cells with high TIM3 and PD-L1 expression. Overstimulating type I IFN signaling may be detrimental in tumors with preexisting high IFN signatures, such as the MC38 model (40–42). Future studies with more tumor models are needed. Nevertheless, the mechanism of action of type I IFNs is complex and warrants careful consideration in the clinic for indication and patient selection.

Alum + ABP-IFNα also had stronger resistance to rechallenge over alum + ABP-IFNβ after B16F10 tumors were cured from IFNs combined with αPD1. More research is needed to explain the mechanism behind the reduced rechallenge efficacy from αPD1 + alum + ABP-IFNβ. As one hypothesis, others have reported that overstimulation of IFN signaling can harm response to αPD1 therapy (28–30) or MPEC formation (77). Although all IFNs achieved high cure rates from αPD1 at the primary tumor, the reduced resistance to rechallenge for alum + ABP-IFNβ reflects inferior adaptive immunity from excessive type I IFN signaling.

In general, alum + ABP-IFNα achieved strong antitumor responses in a variety of contexts and may be a more widely applicable therapy. Alum + ABP-IFNβ can have added benefit, but its use is better reserved for contexts where extra IFN signaling is specifically warranted. More studies that compare type I IFN subtypes will be useful. Reducing our alum + ABP-IFN dose from three doses to one dose may provide further insight into an effective compromise between brief and sustained signaling. Ultimately, rational design of type I IFN signaling strength, local retention, and temporal dynamics holds great promise for controlling effective antitumor immunity.

Materials and Methods

Mice. C57BL/6 mice (Taconic C57BL/6NTac and JAX C57BL/6J) were purchased. $Ifnar1^{-/-}$ (JAX 032045), $Batf3^{-/-}$ (JAX 013755), and $Nlrp3^{-/-}$ mice (JAX 021302) were purchased and bred in-house. Six- to 10-wk old females were used in experiments. All animal work was conducted under the approval of the Massachusetts Institute of Technology Committee on Animal Care in accordance with federal, state, and local guidelines.

Cells. B16F10 (American Type Culture Collection [ATCC]), MC38 (a gift from J. Schlom, National Cancer Institute, Bethesda, MD), B16F10 Trp2KO (generated previously) (78), and RAW-Lucia ISG (InvivoGen) cells were cultured in Dulbecco's modified Eagle's medium (DMEM) (ATCC) supplemented with 10% fetal bovine serum. RAW-Lucia ISG cells were maintained with 200 μg/mL Zeocin (InvivoGen) every other passage. Adherent cells were cultured at 37 °C and 5% CO_2. HEK293-F cells (Gibco) were cultured in FreeStyle293 Expression Medium (Gibco) shaking at 37 °C and 8% CO_2. All cell lines tested negative for mycoplasma.

Cloning and Protein Purification. Murine IFNα, IFNβ, MSA-IFNα, ABP-IFNα, ABP-IFNβ, and human IFNα, ABP-IFNα, were cloned with 6-His tags into the gWiz vector (Genlantis) using In-Fusion cloning (Takara Bio) (*SI Appendix*, Table S1). Fam20C kinase with a KDEL tag (22) and MSA-IL2 with a 6-His tag (47) were previously cloned into the gWiz vector. αPD1 was cloned into the gWiz vector starting with the sequence of 29F.1A12, which was a generous gift from the G. Freeman Laboratory (Dana-Farber Cancer Institute, Boston, MA) (79,80). This clone is typically used in the rat IgG2a format, but we cloned it with a murine IgG2c isotype with a kappa light chain and the LALA-PG mutations to ablate Fc effector functions and prevent target cell clearance (81). Plasmids were amplified in Stellar cells and purified using NucleoBond Xtra endotoxin-free kits (Macherey-Nagel). For transfections, 1 mg plasmid DNA with 2 mL polyethylenimine (Polysciences 23966) in 40 mL OptiPRO Serum Free Medium (Thermo Fisher) was added dropwise to 1 L HEK293-F cells. For ABP-IFNs, the 1 mg plasmid DNA was a mixture of 950 μg ABP-IFN plasmid and 50 μg Fam20C plasmid. After 6 d, proteins were purified from cell supernatants using TALON Metal Affinity Resin (Takara Bio) for IFNs and MSA-IL2, and rProtein A Sepharose Fast Flow Resin (Cytiva) for αPD1. ABP-IFNs and MSA-IL2 were further purified by size exclusion chromatography on an ÄKTA fast protein liquid chromatography system (GE Healthcare). Typical yields per 1 L HEK293-F cells for murine IFNs were ∼10 mg IFNα, ∼5 mg IFNβ, ∼20 mg MSA-IFNα, ∼1 mg ABP-IFNα, and ∼1 mg ABP-IFNβ. Proteins were buffer exchanged into TBS (IFNs) or phosphate-buffered saline (PBS) (MSA-IL2 and αPD1) using Amicon filters (EMD Millipore). Proteins were sterile filtered and confirmed for minimal endotoxin (<0.1 EU per dose) using the LAL Chromogenic Endotoxin Quantitation Kit (Pierce). Molecular weight was confirmed by running proteins alongside a Novex Sharp Pre-Stained Protein Standard on a NuPAGE 4 to 12% Bis-Tris gel (Invitrogen) with 2-(*N*-morpholino) ethanesulfonic acid running buffer and SimplyBlue Safe Stain (Life Technologies). Phosphorylation of ABP-IFNs was confirmed by malachite green assay (Pierce Phosphoprotein Phosphate Estimation Assay Kit). Proteins were flash frozen in liquid nitrogen and stored at −80 °C.

In Vitro Alum Binding. All alum used in this paper was Alhydrogel (InvivoGen vac-alu-250). To fluorescently label proteins, IFNs were incubated with AF647 N-hydroxysuccinimide ester (Invitrogen A20006) in PBS with 0.1 M K_2HPO_4, pH 9 for 2 h at room temperature. Free dye was removed using PD SpinTrap G-25 columns (Cytiva). Fluorescently labeled IFNs (1 μg) and alum (10 μg) were incubated for 20 min in TBS, pelleted, then resuspended in PBS 10% mouse serum for 1 h. Alum was pelleted by centrifugation at 15,000 × *g* to separate the alum-bound fraction from the released fraction, and fluorescence was measured by a Tecan Infinite M200 Pro.

In Vitro Macrophage Activation. RAW-Lucia ISG cells were seeded onto 96-well tissue culture plates at 100,000 cells per well in 200 μL media and varying concentrations of IFNs. For some wells, alum and ABP-IFNs were first mixed at a 5:1 (wt/wt) ratio for 20 min. After 18 h, luciferase levels in cell supernatants were assayed using QUANTI-Luc (InvivoGen) and a Tecan Infinite M200 Pro with an injector, following vendor instructions.

In Vivo Imaging System. IFNs were fluorescently labeled as described above. AF647-labeled and unlabeled IFNs were mixed such that each dose contained 0.5 nmol IFN and 0.1 nmol dye in 20 μL TBS. Low dye levels can minimize quenching artifacts. ABP-IFN groups included 60 μg alum in the dose. On day 0, C57BL/6 mice given alfalfa-free feed were inoculated with 1 M B16F10 Trp2KO cells subcutaneously (s.c.) in the right flank. On day 5, tumors were treated (i.t.).

Fluorescence at the tumor was imaged by in vivo imaging system (IVIS) (PerkinElmer) using a 640-nm excitation filter and 680-nm emission filter. Image analysis was done by Living Image software. Data were normalized to the maximum signal throughout the experiment for each IFN. On days 7 and 10, serum was collected. On day 10, mice were killed and organs were homogenized in tubes containing zirconium beads (Benchmark Scientific) using a minibeadbeater (BioSpec Products) in PBS with 1 mg/mL collagenase/dispase (Roche) and 25 μg/mL DNase I (Roche). Fluorescence in serum and homogenized organs was measured on a Tecan Infinite M200 Pro. Standard curves were generated using serum and organs from untreated mice with AF647-IFNs added ex vivo.

Tumor Treatments and Survival. On day 0, mice were inoculated with 1 M B16F10 or MC38 cells in 50 μL PBS s.c. in the right flank. Treatments began on day 5 when tumors were established (average 24 mm^2 for B16F10 and 30 mm^2 for MC38). Mice were sorted so groups had equal average tumor area at the start of treatment. IFNs were always treated at 0.5 nmol (10 μg IFNα; 10 μg IFNβ; 43 μg MSA-IFNα; 12 μg ABP-IFNα; 12 μg ABP-IFNβ), based on prior IFNα treatments in the laboratory at this dose (54). I.t. doses were in 20 μL TBS. ABP-IFN doses also contained 60 μg alum and were incubated at room temperature for at least 20 min before treatment. Systemic MSA-IFNα was treated i.p. in 100 μL PBS. IFNs were dosed on days 5, 11, and 17, except for the BM chimera study where IFNs were treated on days 6, 12, and 18. For the alum only study, 120 μg alum in 20 μL was treated i.t. on days 5, 7, and 9. MSA-IL2 (30 μg in 50 μL PBS) and αPD1 (200 μg in 100 μL PBS) were treated i.p. on days 5, 11, and 17. Depleting antibodies aCD8α (Bio X Cell 2.43), aNK1.1 (Bio X Cell PK136), and aLy6G (Bio X Cell 1A8) were dosed at 400 μg i.p. every 4 d from day 3 until day 30. Tumor area (length × width) and body weight were monitored. Most survival data are compiled from multiple experiments. Mice were killed when tumors exceeded 100 mm^2, weight loss exceeded 20%, or mice exhibited poor body condition. Mice who died from tumor burden (as defined by the most recent tumor measurement exceeding 70 mm^2) were included in the data. Any other unexpected deaths were omitted from the study. For rechallenge studies, mice were inoculated with 0.1 M B16F10 cells (s.c.) in the left flank at days 100 to 110. Mice were monitored for an additional 100 d and killed when their rechallenge tumor exceeded 100 mm^2.

Bone Marrow Chimeric Mice. Host mice ($CD45.2^+$) were irradiated with 500 rad, allowed to recover for 3 h, and irradiated again with 550 rad. The next day, femurs and tibias were excised from congenically marked donor mice ($CD45.1^+$), and the ends of the bones were cut. BM was harvested by centrifugation at 2,500 × *g*, 70-μm filtered, then washed and resuspended in PBS. The 7.5 M BM cells were injected retroorbitally into irradiated host mice within 24 h postirradiation. Engraftments were confirmed after 6 wk.

Tumor Lysates. Tumors were excised, weighed, and ground with a pestle in 1:20 (wt/vol) of tumor in Tissue Protein Extraction Reagent (Thermo Fisher) supplemented with Halt Protease Inhibitor Mixture (Thermo Fisher) and 5 mM ethylenediaminetetraacetic acid (EDTA). Samples were incubated for 30 min at 4 °C, debris was pelleted by centrifugation at 10,000 × *g*, and supernatants were filtered through Corning Costar Spin-X tubes. The LEGENDplex mouse antivirus response panel (13-plex) (BioLegend) was used following vendor instructions and analyzed with BD FACS LSR Fortessa.

Flow Cytometry. Blood was collected by cheek bleed into K2 EDTA tubes (MiniCollect). Tumors, tdLNs, and spleens were excised, weighed, mechanically dissociated, and 70-μm filtered into single-cell suspensions. Spleens and blood were resuspended in ACK lysing buffer (Gibco). Cells were blocked with CD16/CD32 antibody (eBioscience Clone 93). For intracellular markers, cells were fixed and stained in permeabilization buffer (Invitrogen). Some tumors were stained with Zombie NIR (BioLegend 423105), Apotracker Green (BioLegend 427402), BUV395-CD45 (BD Biosciences 30-F11), AF647-TA99 (labeled in-house), PE/Cy7-MHC-I (BioLegend 28-8-6), PE-PD-L1 (BioLegend 10F.9G2), and BV605-Ki67 (BioLegend 16A8). Other tumors were stained with Zombie UV (BioLegend 423107), BUV395-CD45, BV785-CD3 (BioLegend 17A2), BUV737-CD8α (BD Biosciences 53-6.7), BV605-Ki67, BV711-TIM3 (BioLegend RMT3-23), and AF488-TCF1/TCF7 (Cell Signaling Technology C63D9). Other tumors were stained with Zombie Aqua (BioLegend 423101), BUV395-CD45, PE/Cy7-CD3, BUV737-CD8α, APC-PD-L1, PE-TIM3, and FITC-PD1 (BioLegend 29F.1A12). tdLNs were stained with Zombie NIR, BUV395-CD45, PE/Cy7-Ly6C (BioLegend HK1.4), AF647-MHCII (BioLegend M5/114.15.2), BV605-CD24 (BioLegend M1/69), and PE-CD86 (BioLegend GL-1). Spleens were stained with Zombie Aqua, BUV395-CD45, PE/Cy7-CD3, and BUV737-CD8α. Spleens were also stained with BV605-CD44 (BioLegend IM7), PE-CD127 (BioLegend A7R34), and APC-KLRG1 (BioLegend 2F1) in one panel, and AF647-CD25 (BioLegend PC61), BV605-Ki67, PE-TIM3, and AF488-TCF1/TCF7 in a separate panel. To confirm BM engraftment, blood was stained with Zombie Aqua, APC-CD45.1 (BioLegend A20), and PE-CD45.2 (BioLegend 104). To confirm antibody-mediated depletions, blood was stained with Zombie Aqua, BUV395-CD45, BV785-CD3, BUV737-CD8α, BV711-Ly6G (BioLegend 1A8), APC/Cy7-Ly6C (BioLegend HK1.4), BV421-CD11b (BioLegend M1/70), and PE/Cy7-NKp46 (BioLegend 29A1.4). BD FACS LSR Fortessa or BD FACS Symphony A3 analyzers were used. Data were analyzed with FlowJo V10.

Statistical Analysis. Statistics were performed with GraphPad Prism software V7. Survival was compared by log-rank Mantel–Cox text. As described in figure captions, other metrics were compared by one-way or two-way analysis of variance (ANOVA) with Tukey's multiple comparisons test, or unpaired *t* test. The *n* and *P* values are indicated in the legends.

Data, Materials, and Software Availability. All study data are included in the article and/or supporting information.

ACKNOWLEDGMENTS. This work was supported by the National Cancer Institute Grant 5R01CA174795-03 (to K.D.W.), the National Institute of Biomedical Imaging and Bioengineering Grant 1R01EB031082-01A1 (to D.J.I. and K.D.W.), and the Koch Institute Frontier Research Program via the Casey and Family Foundation Cancer Research Fund (to S.S. and K.D.W.). We were supported by the NSF Graduate Research Fellowship Program (E.A.L., N.M., S.C.C., J.R.P., A.S., B.M.L., and A.M.R.), NIH/National Institute of General Medical Sciences Biotechnology Training Program (E.A.L., N.M., and A.M.R.), Siebel Scholar Award (E.A.L. and N.M.), and a fellowship from the Ludwig Center at the Koch Institute (Y.A.). We were also supported by the Hope Babette Tang Student Research Fund, the Kristin R. Pressman and Jessica J. Pourian Koch Institute Fund, and the Charles S. Krakauer Fund (E.A.L.). We thank the Koch Institute's Robert A. Swanson (1969) Biotechnology Center (National Cancer Institute Grant P30-CA14051) for technical support, specifically the Flow Cytometry Core Facility and Preclinical Imaging and Testing.

Author affiliations: [a]Koch Institute for Integrative Cancer Research, Massachusetts Institute of Technology, Cambridge, MA 02139; [b]Department of Biological Engineering, Massachusetts Institute of Technology, Cambridge, MA 02139; [c]Department of Chemical Engineering, Massachusetts Institute of Technology, Cambridge, MA 02139; [d]Department of Biology, Massachusetts Institute of Technology, Cambridge, MA 02139; [e]Department of Materials Science and Engineering, Massachusetts Institute of Technology, Cambridge, MA 02139; [f]Ragon Institute of Massachusetts General Hospital, Massachusetts Institute of Technology and Harvard University, Cambridge, MA 02139; [g]Consortium for HIV/AIDS Vaccine Development, The Scripps Research Institute, La Jolla, CA 92037; and [h]HHMI, Chevy Chase, MD 20815

1. E. C. Borden, Interferons α and β in cancer: Therapeutic opportunities from new insights. *Nat. Rev. Drug Discov.* **18**, 219–234 (2019).
2. M. Musella, G. Manic, R. De Maria, I. Vitale, A. Sistigu, Type-I-interferons in infection and cancer: Unanticipated dynamics with therapeutic implications. *OncoImmunology* **6**, e1314424 (2017).
3. M. B. Fuertes *et al.*, Host type I IFN signals are required for antitumor CD8+ T cell responses through CD8alpha+ dendritic cells. *J. Exp. Med.* **208**, 2005–2016 (2011).
4. M. S. Diamond *et al.*, Type I interferon is selectively required by dendritic cells for immune rejection of tumors. *J. Exp. Med.* **208**, 1989–2003 (2011).
5. L. Corrales, V. Matson, B. Flood, S. Spranger, T. F. Gajewski, Innate immune signaling and regulation in cancer immunotherapy. *Cell Res.* **27**, 96–108 (2017).
6. J. R. Quesada, J. Reuben, J. T. Manning, E. M. Hersh, J. U. Gutterman, Alpha interferon for induction of remission in hairy-cell leukemia. *N. Engl. J. Med.* **310**, 15–18 (1984).
7. A. M. Eggermont *et al.*; EORTC Melanoma Group, Adjuvant therapy with pegylated interferon alfa-2b versus observation alone in resected stage III melanoma: Final results of EORTC 18991, a randomised phase III trial. *Lancet* **372**, 117–126 (2008).
8. T. M. Herndon *et al.*, U.S. Food and Drug Administration Approval: Peginterferon-alfa-2b for the adjuvant treatment of patients with melanoma. *Oncologist* **17**, 1323–1328 (2012).
9. P. G. Holder *et al.*, Engineering interferons and interleukins for cancer immunotherapy. *Adv. Drug Deliv. Rev.* **182**, 114112 (2022).
10. C. Xuan, K. K. Steward, J. M. Timmerman, S. L. Morrison, Targeted delivery of interferon-alpha via fusion to anti-CD20 results in potent antitumor activity against B-cell lymphoma. *Blood* **115**, 2864–2871 (2010).
11. Y. Liang *et al.*, Targeting IFNα to tumor by anti-PD-L1 creates feedforward antitumor responses to overcome checkpoint blockade resistance. *Nat. Commun.* **9**, 4586 (2018).

12. X. Yang *et al.*, Targeting the tumor microenvironment with interferon-β bridges innate and adaptive immune responses. *Cancer Cell* **25**, 37–48 (2014).
13. G. Garcin *et al.*, High efficiency cell-specific targeting of cytokine activity. *Nat. Commun.* **5**, 3016 (2014).
14. A. Cauwels *et al.*, Delivering type I interferon to dendritic cells empowers tumor eradication and immune combination treatments. *Cancer Res.* **78**, 463–474 (2018).
15. X. Cao *et al.*, Next generation of tumor-activating type I IFN enhances anti-tumor immune responses to overcome therapy resistance. *Nat. Commun.* **12**, 5866 (2021).
16. H. Wang *et al.*, Enzyme-activatable interferon-poly(α-amino acid) conjugates for tumor microenvironment potentiation. *Biomacromolecules* **20**, 3000–3008 (2019).
17. Z. Wang *et al.*, Thermoresponsive and protease-cleavable interferon-polypeptide conjugates with spatiotemporally programmed two-step release kinetics for tumor therapy. *Adv. Sci. (Weinh.)* **6**, 1900586 (2019).
18. R. A. Sheth *et al.*, Assessment of image-guided intratumoral delivery of immunotherapeutics in patients with cancer. *JAMA Netw. Open* **3**, e207911 (2020).
19. R. H. I. Andtbacka *et al.*, Talimogene laherparepvec improves durable response rate in patients with advanced melanoma. *J. Clin. Oncol.* **33**, 2780–2788 (2015).
20. S. Champiat *et al.*, Intratumoral immunotherapy: From trial design to clinical practice. *Clin. Cancer Res.* **27**, 665–679 (2021).
21. N. Momin *et al.*, Anchoring of intratumorally administered cytokines to collagen safely potentiates systemic cancer immunotherapy. *Sci. Transl. Med.* **11**, eaaw2614 (2019).
22. Y. Agarwal *et al.*, Intratumourally injected alum-tethered cytokines elicit potent and safer local and systemic anticancer immunity. *Nat. Biomed. Eng.* **6**, 129–143 (2022).
23. R. Danielli *et al.*, Intralesional administration of L19-IL2/L19-TNF in stage III or stage IVM1a melanoma patients: Results of a phase II study. *Cancer Immunol. Immunother.* **64**, 999–1009 (2015).
24. R. M. Spaapen *et al.*, Therapeutic activity of high-dose intratumoral IFN-β requires direct effect on the tumor vasculature. *J. Immunol.* **193**, 4254–4260 (2014).
25. C. Rozera *et al.*, Interferon (IFN)-β gene transfer into TS/A adenocarcinoma cells and comparison with IFN-α: Differential effects on tumorigenicity and host response. *Am. J. Pathol.* **154**, 1211–1222 (1999).
26. M. Ohashi *et al.*, Adenovirus-mediated interferon alpha gene transfer induces regional direct cytotoxicity and possible systemic immunity against pancreatic cancer. *Br. J. Cancer* **93**, 441–449 (2005).
27. K. Narumi *et al.*, Administration route-dependent induction of antitumor immunity by interferon-alpha gene transfer. *Cancer Sci.* **101**, 1686–1694 (2010).
28. N. Jacquelot *et al.*, Sustained Type I interferon signaling as a mechanism of resistance to PD-1 blockade. *Cell Res.* **29**, 846–861 (2019).
29. J. L. Benci *et al.*, Tumor interferon signaling regulates a multigenic resistance program to immune checkpoint blockade. *Cell* **167**, 1540–1554.e12 (2016).
30. J. L. Benci *et al.*, Opposing functions of interferon coordinate adaptive and innate immune responses to cancer immune checkpoint blockade. *Cell* **178**, 933–948.e14 (2019).
31. N. Momin *et al.*, Maximizing response to intratumoral immunotherapy in mice by tuning local retention. *Nat. Commun.* **13**, 109 (2022).
32. G. Schreiber, J. Piehler, The molecular basis for functional plasticity in type I interferon signaling. *Trends Immunol.* **36**, 139–149 (2015).
33. L. E. Fox, M. C. Locke, D. J. Lenschow, Context is key: Delineating the unique functions of IFNα and IFNβ in disease. *Front. Immunol.* **11**, 606874 (2020).
34. C. Thomas *et al.*, Structural linkage between ligand discrimination and receptor activation by type I interferons. *Cell* **146**, 621–632 (2011).
35. V. van Pesch, H. Lanaya, J.-C. Renauld, T. Michiels, Characterization of the murine alpha interferon gene family. *J. Virol.* **78**, 8219–8228 (2004).
36. H.-Y. Tao, R.-Q. Wang, W.-J. Sheng, Y.-S. Zhen, The development of human serum albumin-based drugs and relevant fusion proteins for cancer therapy. *Int. J. Biol. Macromol.* **187**, 24–34 (2021).
37. G. M. Subramanian, M. Fiscella, A. Lamousé-Smith, S. Zeuzem, J. G. McHutchison, Albinterferon alpha-2b: A genetic fusion protein for the treatment of chronic hepatitis C. *Nat. Biotechnol.* **25**, 1411–1419 (2007).
38. G. L. Morefield *et al.*, Effect of phosphorylation of ovalbumin on adsorption by aluminum-containing adjuvants and elution upon exposure to interstitial fluid. *Vaccine* **23**, 1502–1506 (2005).
39. T. J. Moyer *et al.*, Engineered immunogen binding to alum adjuvant enhances humoral immunity. *Nat. Med.* **26**, 430–440 (2020).
40. S. I. S. Mosely *et al.*, Rational selection of syngeneic preclinical tumor models for immunotherapeutic drug discovery. *Cancer Immunol. Res.* **5**, 29–41 (2017).
41. E. Duong *et al.*, Type I interferon activates MHC class I-dressed CD11b^{+} conventional dendritic cells to promote protective anti-tumor CD8^{+} T cell immunity. *Immunity* **55**, 308–323.e9 (2022).
42. M. G. Lechner *et al.*, Immunogenicity of murine solid tumor models as a defining feature of in vivo behavior and response to immunotherapy. *J. Immunother.* **36**, 477–489 (2013).
43. Y. E. Latchman *et al.*, PD-L1-deficient mice show that PD-L1 on T cells, antigen-presenting cells, and host tissues negatively regulates T cells. *Proc. Natl. Acad. Sci. U.S.A.* **101**, 10691–10696 (2004).
44. B. Diskin *et al.*, PD-L1 engagement on T cells promotes self-tolerance and suppression of neighboring macrophages and effector T cells in cancer. *Nat. Immunol.* **21**, 442–454 (2020).
45. F. Vignaux, I. Gresser, Differential effects of interferon on the expression of H-2K, H-2D, and Ia antigens on mouse lymphocytes. *J. Immunol.* **118**, 721–723 (1977).
46. S. C. Eisenbarth, O. R. Colegio, W. O'Connor, F. S. Sutterwala, R. A. Flavell, Crucial role for the Nalp3 inflammasome in the immunostimulatory properties of aluminium adjuvants. *Nature* **453**, 1122–1126 (2008).
47. E. F. Zhu *et al.*, Synergistic innate and adaptive immune response to combination immunotherapy with anti-tumor antigen antibodies and extended serum half-life IL-2. *Cancer Cell* **27**, 489–501 (2015).
48. D. S. Chen, I. Mellman, Oncology meets immunology: The cancer-immunity cycle. *Immunity* **39**, 1–10 (2013).
49. A. Tzeng *et al.*, Temporally programmed CD8α^{+} DC activation enhances combination cancer immunotherapy. *Cell Rep.* **17**, 2503–2511 (2016).
50. A. M. Rothschilds, K. D. Wittrup, What, why, where, and when: Bringing timing to immuno-oncology. *Trends Immunol.* **40**, 12–21 (2019).
51. M. B. Atkins *et al.*, Randomized phase II trial of high-dose interleukin-2 either alone or in combination with interferon alfa-2b in advanced renal cell carcinoma. *J. Clin. Oncol.* **11**, 661–670 (1993).
52. D. F. McDermott *et al.*, Randomized phase III trial of high-dose interleukin-2 versus subcutaneous interleukin-2 and interferon in patients with metastatic renal cell carcinoma. *J. Clin. Oncol.* **23**, 133–141 (2005).
53. S. Negrier *et al.*, Recombinant human interleukin-2, recombinant human interferon alfa-2a, or both in metastatic renal-cell carcinoma. Groupe Français d'Immunothérapie. *N. Engl. J. Med.* **338**, 1272–1278 (1998).
54. A. Rothschilds *et al.*, Order of administration of combination cytokine therapies can decouple toxicity from efficacy in syngeneic mouse tumor models. *OncoImmunology* **8**, e1558678 (2019).
55. S. A. Rosenberg *et al.*, Prospective randomized trial of the treatment of patients with metastatic melanoma using chemotherapy with cisplatin, dacarbazine, and tamoxifen alone or in combination with interleukin-2 and interferon alfa-2b. *J. Clin. Oncol.* **17**, 968–975 (1999).
56. A. Amouzegar, M. Chelvanambi, J. N. Filderman, W. J. Storkus, J. J. Luke, STING agonists as cancer therapeutics. *Cancers (Basel)* **13**, 2695 (2021).
57. S. M. Kaech *et al.*, Selective expression of the interleukin 7 receptor identifies effector CD8 T cells that give rise to long-lived memory cells. *Nat. Immunol.* **4**, 1191–1198 (2003).
58. N. S. Joshi *et al.*, Inflammation directs memory precursor and short-lived effector CD8(+) T cell fates via the graded expression of T-bet transcription factor. *Immunity* **27**, 281–295 (2007).
59. N. S. Joshi, S. M. Kaech, Effector CD8 T cell development: A balancing act between memory cell potential and terminal differentiation. *J. Immunol.* **180**, 1309–1315 (2008).
60. F. Baharom *et al.*, Intravenous nanoparticle vaccination generates stem-like TCF1^{+} neoantigen-specific CD8^{+} T cells. *Nat. Immunol.* **22**, 41–52 (2021).
61. L. K. Selin *et al.*, Memory of mice and men: CD8+ T-cell cross-reactivity and heterologous immunity. *Immunol. Rev.* **211**, 164–181 (2006).
62. V. Kalia *et al.*, Prolonged interleukin-2Ralpha expression on virus-specific CD8+ T cells favors terminal-effector differentiation in vivo. *Immunity* **32**, 91–103 (2010).
63. A. Tzeng, B. H. Kwan, C. F. Opel, T. Navaratna, K. D. Wittrup, Antigen specificity can be irrelevant to immunocytokine efficacy and biodistribution. *Proc. Natl. Acad. Sci. U.S.A.* **112**, 3320–3325 (2015).
64. B. Weide *et al.*, Intralesional treatment of stage III metastatic melanoma patients with L19-IL2 results in sustained clinical and systemic immunologic responses. *Cancer Immunol. Res.* **2**, 668–678 (2014).
65. R. K. Yang *et al.*, Intratumoral hu14.18-IL-2 (IC) induces local and systemic antitumor effects that involve both activated T and NK cells as well as enhanced IC retention. *J. Immunol.* **189**, 2656–2664 (2012).
66. E. E. Johnson *et al.*, Intratumoral immunocytokine treatment results in enhanced antitumor effects. *Cancer Immunol. Immunother.* **57**, 1891–1902 (2008).
67. T. J. Aiken *et al.*, Short-course neoadjuvant in situ vaccination for murine melanoma. *J. Immunother. Cancer* **10**, e003586 (2022).
68. G. W. Bos *et al.*, In situ crosslinked biodegradable hydrogels loaded with IL-2 are effective tools for local IL-2 therapy. *Eur. J. Pharm. Sci.* **21**, 561–567 (2004).
69. Y. Hori, P. J. Stern, R. O. Hynes, D. J. Irvine, Engulfing tumors with synthetic extracellular matrices for cancer immunotherapy. *Biomaterials* **30**, 6757–6767 (2009).
70. D. A. Zaharoff, K. W. Hance, C. J. Rogers, J. Schlom, J. W. Greiner, Intratumoral immunotherapy of established solid tumors with chitosan/IL-12. *J. Immunother.* **33**, 697–705 (2010).
71. K. Xu *et al.*, Injectable hyaluronic acid-tyramine hydrogels incorporating interferon-α2a for liver cancer therapy. *J. Control. Release* **166**, 203–210 (2013).
72. K. Ueda *et al.*, Growth inhibitory effect of an injectable hyaluronic acid-tyramine hydrogels incorporating human natural interferon-α and sorafenib on renal cell carcinoma cells. *Acta Biomater.* **29**, 103–111 (2016).
73. J.-G. Hu *et al.*, Collagen hydrogel functionalized with collagen-targeting IFNA2b shows apoptotic activity in nude mice with xenografted tumors. *ACS Biomater. Sci. Eng.* **5**, 272–282 (2019).
74. Q. Liu *et al.*, Superior antitumor efficacy of IFN-α2b-incorporated photo-cross-linked hydrogels combined with T cell transfer and low-dose irradiation against gastric cancer. *Int. J. Nanomedicine* **15**, 3669–3680 (2020).
75. M. Buttmann, F. Berberich-Siebelt, E. Serfling, P. Rieckmann, Interferon-beta is a potent inducer of interferon regulatory factor-1/2-dependent IP-10/CXCL10 expression in primary human endothelial cells. *J. Vasc. Res.* **44**, 51–60 (2007).
76. R. M. Strieter, J. A. Belperio, R. J. Phillips, M. P. Keane, CXC chemokines in angiogenesis of cancer. *Semin. Cancer Biol.* **14**, 195–200 (2004).
77. M. Wiesel *et al.*, Type-I IFN drives the differentiation of short-lived effector CD8+ T cells in vivo. *Eur. J. Immunol.* **42**, 320–329 (2012).
78. K. D. Moynihan *et al.*, Eradication of large established tumors in mice by combination immunotherapy that engages innate and adaptive immune responses. *Nat. Med.* **22**, 1402–1410 (2016).
79. S. C. Liang *et al.*, Regulation of PD-1, PD-L1, and PD-L2 expression during normal and autoimmune responses. *Eur. J. Immunol.* **33**, 2706–2716 (2003).
80. S. C. Cowles *et al.*, An affinity threshold for maximum efficacy in anti-PD-1 immunotherapy. *mAbs* **14**, 2088454 (2022).
81. M. Lo *et al.*, Effector-attenuating substitutions that maintain antibody stability and reduce toxicity in mice. *J. Biol. Chem.* **292**, 3900–3908 (2017).